Contrib Mineral Petrol (1991) 107:202–218

Contributions to Mineralogy and Petrology

Phase equilibria and melt productivity in the pelitic system: implications for the origin of peraluminous granitoids and aluminous granulites

Alberto E. Patiño Douce* and A. Dana Johnston

Department of Geological Sciences, University of Oregon, Eugene, OR 97403-1272, USA

Received May 7, 1990 / Accepted September 21, 1990

Abstract. Peraluminous granitoid magmas are a characteristic product of ultrametamorphism leading to anatexis of aluminous metasedimentary rocks in the continental crust. The mechanisms and characteristic length-scales over which these magmas can be mobilized depend strongly on their melt fraction, because of their high viscosities. Thus, it is of fundamental importance to understand the controls exerted by pressure, temperature and bulk composition of the source material on melt productivity. We have studied experimentally the vapour-absent melting behaviour of a natural metapelitic rock and our results differ greatly from those of previous experimental and theoretical investigations of melt productivity from metamorphic rocks. Under H_2O-undersaturated conditions, bulk composition of the source material is the overriding factor controlling melt fraction at temperatures on the order of 850–900° C. Granitoid melts formed in this temperature interval by the peritectic dehydration-melting reaction:

Biotite + plagioclase + aluminosilicate + quartz = melt + garnet

have a restricted compositional range. As a consequence, melt fractions will be maximized from protoliths whose modes coincide with the stoichiometry of the melting reaction. This "optimum mode" (approximately 38% biotite, 32% quartz, 22% plagioclase and 8% aluminosilicate) reflects the fact that generation of low-temperature granitoid liquids requires both fusible quartzo-feldspathic components and H_2O (from hydrous minerals). Metapelitic rocks rich in mica and aluminosilicate and poor in plagioclase contain an excess of refractory material (Al_2O_3, FeO, MgO) with low solubility in low-temperature silicic melts, and will therefore be poor magma sources. Melt fraction varies inversely with pressure in the range 7–13 kbar, but the effect is not strong: the decrease (at constant temperature) over this pressure range is of at most 15 vol% (absolute).

The liquids produced in our experiments are silica-rich (68–73 wt% SiO_2), strongly peraluminous (2–5 wt% normative corundum) and very felsic (MgO + FeO* + TiO_2 less than 3 wt%, even at temperatures above 1000° C). The last observation suggests that peraluminous granitoids with more than 10% mafic minerals (biotite, cordierite, garnet) contain some entrained restite. Furthermore, because liquids are also remarkably constant in composition, we believe that restite separation is more important than fractional crystallization in controlling the variability within and among peraluminous granitoids.

We present liquidus phase diagrams that allow us to follow the phase relationships of melting of silica- and alumina-saturated rocks at pressures corresponding to the mid- to deep-continental crust. Garnet, aluminosilicate, quartz and ilmenite are the predominant restitic phases at temperatures of about 900° C, but Ti-rich biotite or calcic plagioclase can also be present, depending on the bulk composition of the protolith. At temperatures above 950–1050° C (depending on the pressure) the restitic assemblage is: hercynitic spinel + ilmenite + quartz ± aluminosilicate. Our results therefore support the concept that aluminous granulites (garnet – spinel – plagioclase – aluminosilicate – quartz) can be the refractory residuum of anatectic events.

Introduction

Anatexis of metamorphic rocks within the continental crust is a process of major petrologic importance, whose products range in scale from centimetre-sized migmatitic segregations to granitoid intrusive complexes cropping out over areas of up to several tens of thousands of square kilometres. It is thus of fundamental importance that we understand the melting behaviour of possible crustal protoliths for granitoid magmas. Aluminous schists and gneisses (primarily of sedimentary derivation) are generally considered to be likely source rocks for

* Now at: Department of Geology, University of Georgia, Athens, GA 30602, USA

Offprint requests to: A.E. Patiño Douce

the strongly peraluminous [1] magmas which are predominant in continental anatectic terranes. Although this link between aluminium-rich, muscovite- and/or biotite-bearing metamorphic rocks and peraluminous granitoids is reasonably well established, we are still largely ignorant of many of the details of the anatectic process. Foremost among these is the behaviour of melt fraction during progressive anatexis, and the way in which the melt fraction depends on variables such as the composition of the protolith, temperature, pressure, and availability and composition of a fluid phase.

A few recent studies have partially addressed the problem of melt production from metamorphic rocks. Vielzeuf and Holloway (1988) carried out a series of vapour-absent melting experiments at 10 kbar on a natural quartz- and plagioclase-rich metapelitic rock. They concluded that the variation of melt fracting during anatexis of dry rocks containing muscovite and biotite is a stepwise function of temperature, largely defined by two almost-isothermal melting reactions: the muscovite and biotite dehydration-melting reactions. A notable result of these authors was the large melt fraction (about 60 wt%) observed at temperatures of 875–900° C. Le Breton and Thompson (1988) studied the melting behaviour of biotite-plagioclase-aluminosilicate-quartz assemblages at 10 kbar and estimated melt fractions in the range 6–16 wt% at 860° C. Peterson and Newton (1989) studied melting of non-peraluminous biotite-quartz-feldspar assemblages over a wide range of pressures and water contents. They estimated that, at 10 kbar, vapour-absent melting of biotite + quartz produces no more than 20–30 vol% melt at the solidus (about 850° C). Vapour-absent melting in a somewhat different system (biotite-hornblende tonalite) was studied by Rutter and Wyllie (1988), who also suggested the stepwise nature of melting in systems containing multiple hydrous phases. Finally, Clemens and Vielzeuf (1987) proposed a theoretical model for calculating melt fraction as a function of temperature and hydrous-mineral content of the protolith.

In this contribution we present the results of an experimental study designed to elucidate the variation of melt fraction during progressive vapour-absent melting (dehydration-melting) of aluminous metasediments. Our results differ in several important respects from those of some of the studies cited above. We have not observed a stepwise increase in melt fraction but, rather, a smooth increase in melt fraction with temperature. The biotite dehydration-melting reaction takes place in our experiments over a temperature interval of at least 150° C, in contrast with the almost-isothermal reaction described by Vielzeuf and Holloway (1988). Furthermore, even though our starting material contains about 50% more hydrous minerals than that studied by Vielzeuf and Holloway, the melt fractions produced in our experiments over the temperature range 850–1050° C are considerably lower (by up to 50% relative) than those reported by these authors. An important corollary is that inferring melt productivity of metasediments from their hydrous-mineral content alone is in general not warranted and that maximum melt production should be expected from metagraywackes and not from mica-rich and plagioclase-poor metapelites.

[1] We adopt here the terminology proposed by Miller (1985) considering a granitoid rock to be strongly peraluminous if its equilibrium mineral assemblage contains one or more alumina-saturating phases, such as muscovite, andalusite, sillimanite, cordierite or garnet

Generalized phase relationships of melting of metamorphic rocks

The relationships between dehydration-melting, vapour-saturated melting and subsolidus dehydration of a rock containing a hydrous-mineral phase are shown in a generalized fashion in Fig. 1, which is redrawn after Thompson and Algor (1977), where the reader is referred for a more detailed discussion. For this discussion, we label any assemblage containing a hydrous mineral (mica or amphibole) H, while A represents any assemblage composed exclusively of anhydrous phases. Considered together, curves 1 and 3 are the water-saturated solidus of the rock, along which an H_2O-saturated melt, M_S is formed. Curve 2 is the solidus of the rock under vapour-absent conditions, at pressures in excess of the invariant point, I. Along this curve, which corresponds to the dehydration-melting reaction, the hydrous-mineral-bearing assemblage melts to a hydrous, but H_2O-undersaturated melt (M_u), plus an anhydrous-mineral assemblage, without a vapour phase ever being present. Subsolidus dehydration takes place along curve 4, where an assemblage containing a hydrous mineral reacts to form an anhydrous assemblage plus H_2O vapour. In the simplified system $K_2O-Al_2O_3-SiO_2-H_2O$ (KASH), these curves are univariant and intersect at an invariant point whose pressure is the minimum

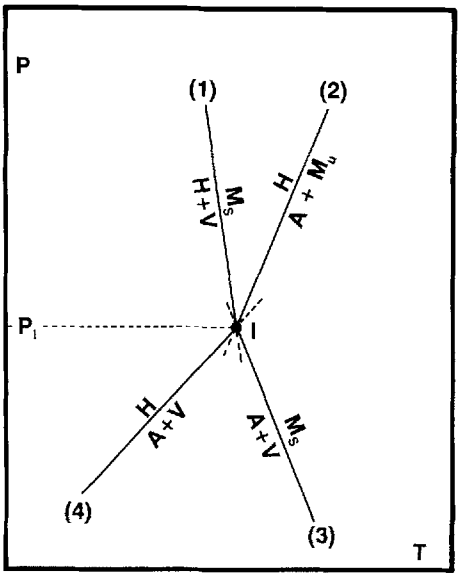

Fig. 1. Generalized pressure-temperature diagram showing the relationships between dehydration-melting (*curve 2*), vapour-saturated melting (*curves 1, 3*) and subsolidus dehydration (*curve 4*). Hydrous minerals cannot coexist stably with melt at pressures lower than P_I

Table 1. Characterization of HQ-36 starting material

	Modal proportion	SiO_2	Al_2O_3	TiO_2	FeO*	MnO	MgO	CaO	Na_2O	K_2O	F	H_2O	Total
Bulk rock[a]	–	57.36	23.24	1.26	8.59	0.17	2.72	0.40	0.48	3.63	0.11	1.69	99.65
Quartz	31	-	–	–	–	–	–	–	–	–	–	–	–
Biotite	30	34.68	19.53	2.68	20.84	0.11	8.13	0.00	0.29	8.92	0.31	4.51[b]	100.00
Aluminosilicate	19	–	–	–	–	–	–	–	–	–	–	–	–
Muscovite	10	46.57	36.63	0.86	1.09	0.02	0.67	0.02	0.96	9.56	0.12	3.51[b]	100.00
Plagioclase	4	65.52	24.96	–	0.02	–	–	5.55	8.31	0.08	-	–	101.44
Garnet	5	36.76	20.97	0.01	34.44	2.82	3.64	1.23	–	–	–	–	99.94
Ilmenite	1	0.07	0.02	52.20	45.50	1.10	0.18	0.01	–	–	-	–	99.08

All values in wt%. Probe analyses of minerals are averages of 8–12 different crystals. Modal proportions calculated by mass balance

[a] Analyzed by XRF except Na by instrumental neutron-activation analysis and F and H_2O calculated from modal proportion of micas

[b] Calculated by difference

pressure at which dehydration-melting can occur or, equivalently, the minimum pressure at which the hydrous mineral considered can coexist stably with melt (H_2O-saturated or undersaturated). In rocks containing several hydrous minerals, all of these minerals begin to react out together and dehydration melting takes place continuously over a multivariant temperature-pressure interval. Thus, we will show that in the rock that we studied, which contains muscovite and biotite, the muscovite dehydration-melting reaction, which defines the vapour-absent solidus of the rock, involves reaction of biotite as well. Once muscovite is exhausted, the biotite dehydration-melting reaction progresses in a continuous fashion from the muscovite-out temperature to the biotite-out temperature.

In order to use these phase relationships as a means of increasing our understanding of crustal anatexis, it is best to consider two end-member situations: H_2O-saturated melting along curve (1) and dehydration melting of a vapour-free rock along curve (2). Water saturated melting would constitute the most favourable situation for melt generation. If a rock containing free vapour begins to melt isobarically along curve 1, however, it will continue melting only as long as the vapour available is sufficient to saturate the amount of melt produced. The large solubility of H_2O in silicic melts under pressure (about 10 wt% at 10 kbar, e.g. Burnham 1979) casts serious doubts on whether this process is capable of generating melt fractions in excess of 5 or 10%, because the amount of free H_2O required is seldom present in the mid- to deep-continental crust. Furthermore, the negative dP/dT slope of the water-saturated solidus would prevent such melts from ascending without freezing. Melts formed under H_2O-saturated conditions would thus tend to form autochthonous (e.g. Didier 1973) granitic massifs and migmatites. Allochthonous granitoids, intruded at crustal levels which are shallower than those at which anatexis took place, must be generated under H_2O-undersaturated conditions.

It is our view that the other end-member situation, dehydration melting of a vapour-free rock along curve 2 (Fig. 1) is a better approximation to the conditions under which crustal anatexis commonly takes place. Our experiments therefore are designed to study dehydration-melting reactions of aluminous metamorphic rocks.

Characterization of the starting material and experimental procedures

All of our experiments utilized the same starting material, a natural metapelitic rock (HQ-36) from northern Idaho (USA), provided by J.M. Rice. The bulk composition of HQ-36, together with its mineral compositions and mode, are presented in Table 1. Sample HQ-36 is representative of a pelitic sediment relatively poor in quartzo-feldspathic clastic components, in contrast with the more psammitic rock studied by Vielzeuf and Holloway (1988). The difference between both rocks is especially conspicuous in their contents of CaO and Na_2O. The mineral assemblage of HQ-36 crystallized under $P-T$ conditions corresponding to the upper-amphibolite facies of Barrovian metamorphism. Rice et al. (1988) have estimated that the peak-metamorphic conditions that affected the area of northern Idaho where HQ-36 crops out were approximately 700° C and 8 kbar.

Experiments were run at 7, 10 and 13 kbar, covering the temperature intervals 825–1075° C at 7 and 10 kbar and 900–1000° C at 13 kbar. Run durations varied from 14 days at the lowest temperatures (< 875° C) to 2 days at the highest temperatures (see Table 2 for run conditions and phase assemblages). All experiments were done in a 0.5-inch piston-cylinder apparatus. Two different kinds of solid-medium cell assemblies were used, an all-NaCl cell up to about 20° C below the melting point of NaCl and, at higher temperatures, a cell with $BaCO_3$ inner parts and a glass sleeve between the graphite furnace and the NaCl outer jacket. The pressures reported are nominal (Heise gauge) pressures and are believed to be accurate to within 0.5 kbar for both cell assemblies (Bohlen 1984). Experiments were pressurized at room temperature to 2 kbar below the target pressure, then heated to the target temperature and the pressure finally adjusted to its nominal value. Because of thermal expansion, this final adjustment corresponded in every case to a pressure release (hot, piston out).

Temperature was measured using $W_{75}-Re_{25}/W_{95}-Re_5$ thermocouples relative to an Omega electronic ice point (0° C) and controlled by a digital Eurotherm 808 temperature controller. Temperature stability throughout all runs was better than ± 5° C. Utilization of small sample volumes (see below) resulted in the entire sample capsule being within 2–3 mm of the thermocouple.

Samples were contained in welded gold capsules. Considerable care was exercised to eliminate as much adsorbed humidity from the starting material as possible. The capsules were filled with 10–15 mg of sample ground to less than 10 µm and pre-dried. The capsules were then stored open in an 130° C oven for at least 24 h

Table 2. Run conditions and phase assemblages

Run no.	Pressure (kbar)	Temperature (°C)	Duration (h)	Cell	Phase assemblage
APD-25	7	825	360	NaCl	Qtz Als Bio Gar Ilm Melt
APD-22	7	850	336	NaCl	Qtz Als Bio Gar Ilm Melt
APD-33	7	875	265	NaCl	Qtz Als Bio Gar Ilm Melt
APD-34	7	900	118	NaCl	Qtz Als Bio Gar Ilm Melt
APD-43	7	950	77	NaCl	Qtz Als Bio Gar Ilm Rut Melt
APD-36	7	975	75	$BaCO_3$	Qtz Als Ilm Spi Melt
APD-39	7	1000	72	$BaCO_3$	Qtz Als Ilm Rut Spi Melt
APD-32	7	1075	48	$BaCO_3$	Qtz Als Ilm Rut Spi Melt
APD-12	10	825	336	NaCl	Qtz Als Bio Gar Ilm Melt
APD-11	10	850	336	NaCl	Qtz Als Bio Gar Ilm Melt
APD-13	10	875	260	NaCl	Qtz Als Bio Gar Ilm Melt
APD-4	10	900	120	NaCl	Qtz Als Bio Gar Ilm Rut Melt
APD-16	10	925	120	NaCl	Qtz Als Bio Gar Rut Melt
APD-9	10	950	75	NaCl	Qtz Als Bio Gar Rut Melt
APD-19	10	975	75	NaCl	Qtz Als Bio Gar Rut Melt
APD-55	10	975	52	$BaCO_3$	Qtz Als Bio Gar Ilm Rut Melt
APD-17	10	1000	72	$BaCO_3$	Qtz Als Gar Rut Melt
APD-24	10	1025	72	$BaCO_3$	Qtz Als Gar Ilm Spi Melt
APD-27	10	1075	48	$BaCO_3$	Qtz Als Gar Ilm Spi Melt
APD-46	13	900	120	NaCl	Qtz Als Bio Gar Rut Melt
APD-44	13	950	74	NaCl	Qtz Als Bio Gar Rut Melt

and then crimped shut inside the oven and immediately sealed by arc-welding. After every run the pressure medium was completely dissolved and the capsule carefully inspected for tears and weighed. If tears or weight loss were detected the run was discarded and repeated.

The absence of a vapour phase in the experiments prevented buffering of the oxygen fugacity. It has been shown that cell assemblies of very similar design to our all-NaCl cell impose an f_{O_2} about 1 log unit above the Ni–NiO buffer (Carroll and Wyllie 1990) although Newton (written communication in review) has found that f_{O_2} in this kind of cell is below QFM. The oxide-mineral assemblage in most of the runs employing this cell [ilmenite (Ilm) solid solution (ss) with haematite $(Hm)_{2-4} \pm$ rutile, Table 2 and Patiño Douce and Johnston, in preparation] shows that the amount of Fe^{3+} in the charges is small, consistent with an oxygen fugacity in the neighbourhood of the QFM buffer. It is noteworthy that a characteristic of many strongly peraluminous granitoids is the occurrence of ilmenite ($\pm$rutile) and the absence of magnetite (e.g. Miller 1985), as observed in the experimental-run products. To compare the oxidation conditions imposed by the $BaCO_3$ cell to those obtained with the NaCl cell, we duplicated a run (975° C, 10 kbar) with both cell assemblies (see Table 2). The composition of the oxide phase in the run with the $BaCO_3$ cell (Ilm ss with Hm_{22}) suggests an oxygen fugacity about 1.5 log units higher than that imposed by the NaCl cell. Small differences are observed in the compositions of biotite, garnet and melt between both runs at the same pressure and temperature (Table 4). These differences, however, are not large enough to affect the modes significantly (Table 5) nor the maximum thermal stability of biotite.

Because none of the experiments were reversed, the attainment of equilibrium cannot be demonstrated rigorously. However, a number of observations support an acceptable approach to equilibrium. Melt compositions and modes were found to change very regularly and consistently throughout the full pressure-temperature range investigated (Tables 4 and 5), and the same is true of biotite, garnet and ilmenite compositions (Patiño Douce and Johnston, in preparation). Also, with the exception of garnet, melt and mineral compositions are notably constant throughout any given charge.

Garnet produced by the dehydration-melting reaction of biotite nucleates around the garnet initially present in the charges but, because of slow cation-diffusion rates, the crystals are not ho-

Table 3. Point-count data of experimental-run products

Temperature (°C)	Qtz	Als	Gar[a]	Bio	Oxi[b]	Spi	Melt
			7 kbar				
825	17	17	4	43	1	0	17
850	17	25	6	28	1	0	22
875	17	21	8	24	1	0	29
900	16	25	13	16	1	0	29
950	2	11	24	3	3	0	57
975	4	14	0	0	6	9	66
1000	4	8	0	0	4	18	65
1075	0	9	0	0	2	18	71
			10 kbar				
825	18	25	4	33	1	0	18
850	23	28	6	28	1	0	23
875	22	21	11	25	1	0	21
900	12	22	17	17	1	0	31
925	5	19	19	20	1	0	35
950	8	18	17	5	2	0	51
975	8	16	14	1	3	0	58
1000	1	18	17	0	3	0	60
1025	1	16	12	0	3	4	63
1075	2	14	5	0	1	12	66
			13 kbar				
900	13	20	16	23	3	0	24
950	4	19	21	11	2	0	42

Point counting was carried out on backscattered-electron photomosaics (see Fig. 2), by superimposing a transparent square grid on the mosaics. Approximately 500 points were counted per mosaic

[a] Garnet cores and rims not distinguished by point counting
[b] Oxi includes all non-spinel oxide phases (ilmenite and rutile)

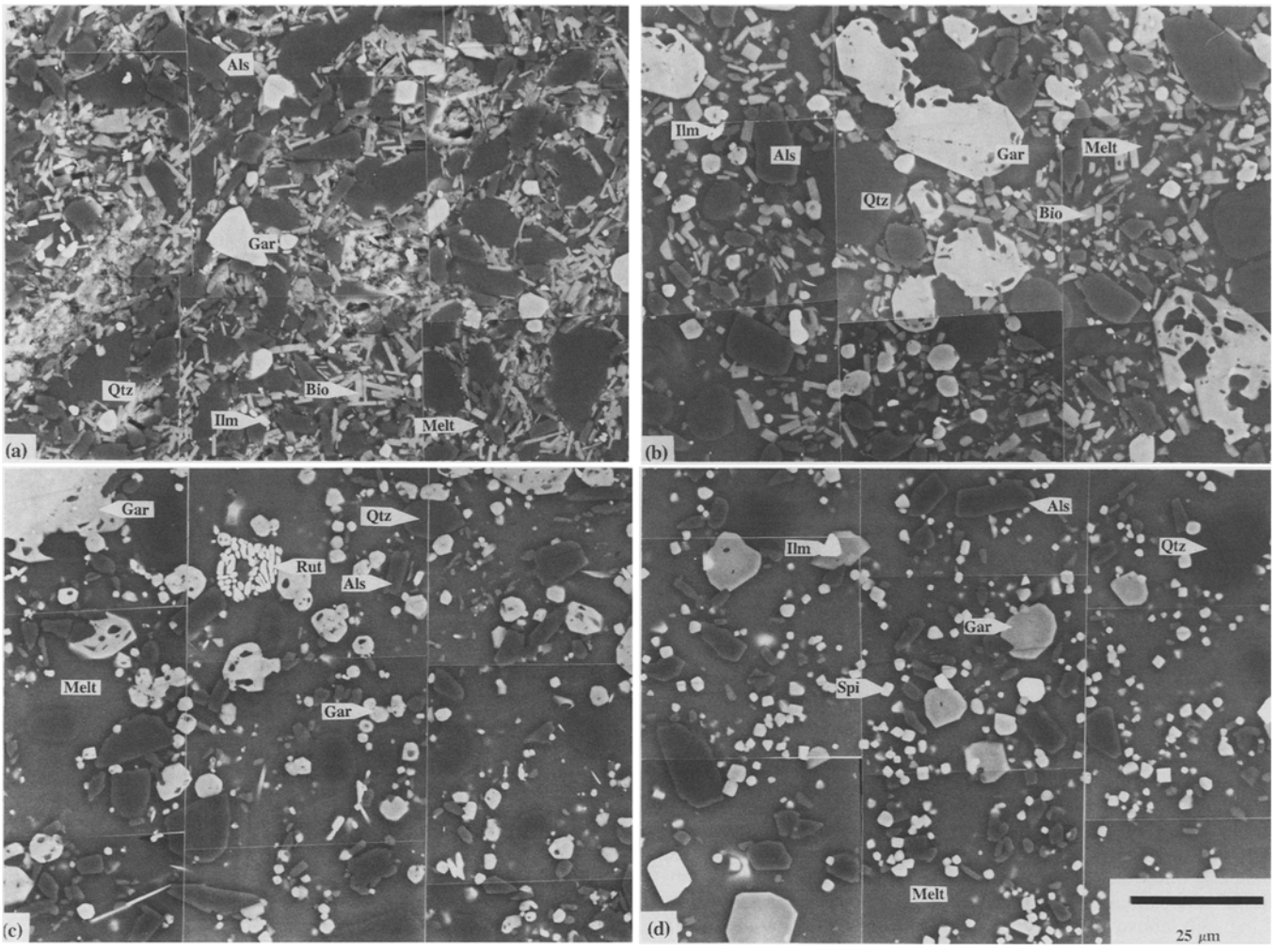

Fig. 2a–d. Backscattered-electron photomosaics of selected 10 kbar run products: **a** 825° C; **b** 900° C; **c** 975° C; **d** 1075° C. Scale bar applies to all mosaics

mogenized and garnet analyses fall into two distinct populations, cores and rims. A similar situation may arise in nature, where zoned garnets are the norm rather than the exception. This may significantly affect the contents of Ca and Mn in natural anatectic melts.

Analytical procedures and mode calculations

All successful run products were mounted in epoxy, sawed in half and polished for electron-beam analysis. A high-resolution backscattered-electron (BSE) photomosaic covering approximately 130×110 μm was prepared for each sample, using a JEOL SM-35 scanning electron microscope equipped with a Robinson BSE detector (Fig. 2). Every phase present in the run products was identified positively by means of energy-dispersive semiquantitative analysis, and each mosaic was point-counted in order to obtain relative-area modal proportions (Table 3).

Potassium counts were corrected for element volatilization using data collected from a time series of analyses[2]. Unfortunately, because of the poor-statistical characteristics displayed by Na counts (particularly at short counting times) this method could not be used to correct Na_2O analyses. We thus decided to discard all Na_2O glass analyses and to calculate the Na_2O content of the glasses by mass balance instead. Our calculated Na_2O values are on the order of double the measured values, underscoring the importance of evaluating critically Na_2O analyses of hydrous glasses. Water content in the glasses was calculated in a similar fashion, by mass balance. The good totals obtained for the glass analyses (Table 4) lend confidence in the procedures that we adopted.

Acquisition of reliable modal data was a fundamental motivation of this study. Given the characteristics of our run products, however, traditional approaches used to determine modal compositions are not entirely satisfactory. Point counting is hampered by the large inhomogeneities in grain size and shape of the run products (Fig. 2), whereas mass-balance calculations with a large number of phases (cf. Table 2) are very sensitive to small inaccuracies in the chemical analyses of the various phases and of the bulk composition. In order to circumvent these difficulties we combined both approaches and calculated modes by optimizing the system:

$$\begin{vmatrix} A \\ C \end{vmatrix} x = \begin{vmatrix} b \\ d \end{vmatrix}$$

where A is a matrix whose columns are the phase compositions, b is the bulk composition of the starting material, C is a matrix whose rows describe the ratios between the total masses of phases with similar grain sizes and shapes (obtained from point counting

[2] Further details of the correction procedure can be obtained from the authors upon request

Table 4. Glass compositions (wt%)

Temperature (°C)	Na_2O	K_2O	MgO	Al_2O_3	SiO_2	FeO*	CaO	MnO	TiO_2	F	P_2O_5	H_2O	Total
						7 kbar							
825	3.18	5.22	0.31	13.56	67.22	1.50	0.55	0.04	0.08	0.05	0.09	3.45	95.25
850	2.23	5.60	0.33	13.34	70.06	1.55	0.30	0.07	0.10	0.00	0.00	5.48	99.06
875	1.77	5.61	0.35	14.85	69.72	1.65	0.35	0.00	0.13	0.01	0.05	4.09	98.58
900	1.32	5.31	0.35	13.72	70.85	1.72	0.24	0.02	0.38	0.11	0.05	3.33	97.40
950	0.87	6.52	0.39	13.84	71.41	1.78	0.15	0.03	0.28	0.16	0.06	3.06	98.56
975	0.85	6.38	0.87	13.14	70.79	1.99	0.39	0.15	0.51	0.11	0.07	2.98	98.22
1000	0.89	6.72	0.66	13.25	70.21	2.14	0.39	0.10	0.61	0.17	0.09	3.13	98.36
1075	0.82	6.23	0.88	12.90	72.95	2.01	0.38	0.13	0.61	0.14	0.07	2.90	100.02
						10 kbar							
825	2.89	5.32	0.45	13.55	69.36	1.62	0.60	0.01	0.02	0.00	0.14	4.67	98.64
850	2.24	5.69	0.41	14.25	70.86	1.70	0.39	0.05	0.13	0.10	0.05	4.33	100.19
875	1.65	6.20	0.37	13.65	70.39	1.62	0.28	0.01	0.17	0.11	0.09	4.72	99.26
900	1.29	6.06	0.41	13.46	71.54	1.61	0.23	0.03	0.21	0.08	0.10	3.47	98.48
925	1.22	6.13	0.37	13.80	71.85	1.60	0.21	0.02	0.26	0.08	0.07	3.23	98.85
950	1.10	6.86	0.33	13.46	73.66	1.65	0.13	0.05	0.37	0.08	0.04	3.55	101.29
975	0.97	6.92	0.49	13.62	73.13	1.74	0.13	0.03	0.37	0.15	0.10	3.49	101.14
975[a]	0.93	6.69	0.86	13.37	70.86	2.93	0.17	0.04	0.42	0.15	0.06	3.38	99.86
1000	0.85	6.40	0.70	13.48	72.63	2.07	0.20	0.04	0.35	0.12	0.08	3.00	99.93
1025	0.79	5.98	1.04	13.40	70.62	3.26	0.26	0.11	0.65	0.10	0.11	2.79	99.12
1075	0.84	6.05	1.09	13.64	69.44	3.04	0.28	0.08	0.73	0.17	0.06	2.95	98.37
						13 kbar							
900	1.79	5.92	0.41	14.14	68.15	1.51	0.21	0.02	0.28	0.11	0.05	7.14	99.74
950	1.21	7.72	0.34	13.51	68.46	1.40	0.10	0.04	0.26	0.12	0.09	5.33	98.57

All elements analyzed with 5 nA beam currents, except Na_2O and H_2O calculated by mass balance. K_2O values corrected as described in text. All values are averages of 5–12 individual analyses

[a] $BaCO_3$ cell assembly

and tabulated densities of the phases), d is 0 and x is the mode in mass%.

We believe that the modal compositions (both mass% and vol%) obtained in this manner (Table 5) are a much better representation of the real modes than the raw point-count data shown in Table 3. The uncertainties in the melt fractions are estimated to be on the order of ±4% (absolute), on the basis of the uncertainties in the chemical analyses and in the point counting.

Variation of melt fraction during progressive anatexis of silica- and alumina-saturated metamorphic rocks

Melt fractions generated in our experiments are plotted in Fig. 3 as a function of temperature and pressure. We divide the melting interval into three segments, corresponding to three melting reactions which, in order of increasing temperature, are:

incongruent melting of muscovite + biotite + quartz ± plagioclase
incongruent melting of biotite + aluminosilicate + quartz ± plagioclase
incongruent melting of garnet + aluminosilicate

The third reaction presupposes that biotite is exhausted before the other reactants in the preceding reaction, as is the case in the composition that we studied.

It is clear from Fig. 3 and Table 5 that the melt productivities of these reactions are quite different. The muscovite reaction is completed below 825° C, and produces about 15 wt% melt. The biotite reaction is responsible for a large increase in melt fraction, but this increase takes place over a temperature interval of about 150° C. Above the biotite-out temperature, melting of refractory phases (garnet + aluminosilicate) is reflected in a very flat section of the melt productivity curve.

Muscovite dehydration-melting reaction

At the lowest temperature that we investigated (825° C) the experimental charge at 10 kbar contains about 15 wt% melt and both muscovite and plagioclase are absent. The amount of quartz present at this temperature is smaller than that contained in the starting material, whereas the abundance of aluminosilicate is greater (see Table 5). Because the biotite content in this run is virtually unchanged relative to that of the starting material (Table 5), it would appear that the following incongruent dehydration-melting reaction occurs below 825° C:

$$[3]\ \mathrm{Mus} + \mathrm{Plg} + \mathrm{Qtz} = \mathrm{Melt} + \mathrm{Als} \qquad (1)$$

[3] See appendix for mineral symbols used in text

Table 5. Modal compositions of experimental run products (calculated by mass balance, see text)

Temperature (°C)	Qtz	Als	Gar(R)[a]	Gar(C)[a]	Bio	Ilm	Rut	Spi	Melt
					a) Wt%				
					7 kbar				
825	26	22	0	6	32	0.5	0.0	0	13
850	21	22	0	9	27	0.1	0.0	0	20
875	19	21	3	9	23	0.2	0.0	0	26
900	13	20	5	8	19	0.2	0.0	0	34
950	1	15	22	5	1	0.1	1.3	0	55
975	12	13	0	0	0	3.6	0.0	16	57
1000	16	9	0	0	0	0.9	0.6	21	54
1075	10	11	0	0	0	2.8	0.0	17	58
					10 kbar				
825	25	22	2	4	31	0.5	0.0	0	15
850	21	21	5	5	27	0.3	0.0	0	19
875	18	20	9	4	21	0.3	0.0	0	27
900	12	19	10	6	18	0.1	0.1	0	35
925	11	18	15	3	14	0.0	0.2	0	38
950	8	18	18	4	7	0.0	0.6	0	43
975	4	17	21	4	2	0.0	0.8	0	49
975[b]	7	19	16	4	3	2.0	0.0	0	49
1000	0	16	19	7	0	0.0	0.8	0	56
1025	2	15	14	4	0	2.3	0.0	2	60
1075	5	15	10	3	0	2.5	0.0	4	61
					13 kbar				
900	19	20	6	9	22	0.0	0.1	0	25
950	12	19	20	3	7	0.0	0.7	0	39
					b) Vol%				
					7 kbar				
825	29	19	0	4	31	0.3	0.0	0	16
850	24	18	0	6	27	0.1	0.0	0	24
875	20	17	2	6	23	0.1	0.0	0	31
900	14	16	4	6	18	0.1	0.0	0	41
950	1	13	16	4	1	0.1	0.8	0	66
975	12	10	0	0	0	2.1	0.0	10	65
1000	17	7	0	0	0	0.5	0.3	14	61
1075	11	9	0	0	0	1.7	0.0	11	68
					10 kbar				
825	28	19	2	3	30	0.3	0.0	0	18
850	24	18	4	4	27	0.2	0.0	0	24
875	20	17	7	3	21	0.2	0.0	0	33
900	13	15	7	4	17	0.1	0.1	0	42
925	12	15	11	2	13	0.0	0.1	0	46
950	9	15	14	3	7	0.0	0.4	0	53
975	5	14	16	3	2	0.0	0.5	0	60
975[b]	8	14	13	3	3	1.2	0.0	0	58
1000	0	13	13	5	0	0.0	0.5	0	68
1025	2	13	10	2	0	1.4	0.0	1	70
1075	6	12	6	2	0	1.5	0.0	3	71
					13 kbar				
900	21	17	4	6	22	0.0	0.0	0	31
950	13	16	15	2	6	0.0	0.4	0	47

[a] (R) and (C) refer to garnet rims and cores, respectively
[b] $BaCO_3$ cell assembly

The melt produced at 825° C, however, contains more H_2O than that which would be expected from muscovite by reaction (1). This can be seen in Fig. 4a, the $K_2O \cdot Al_3O_3 - Na_2O \cdot Al_2O_3 - H_2O$ (KNH) pseudoternary plane of the pseudoquaternary volume $K_2O \cdot Al_2O_3 - Na_2O \cdot Al_2O_3 - (MgO + FeO^*) - H_2O$ (KNMH, Fig. 4b). The composition of HQ-36 projects close to the mica-plagioclase join. If muscovite dehydra-

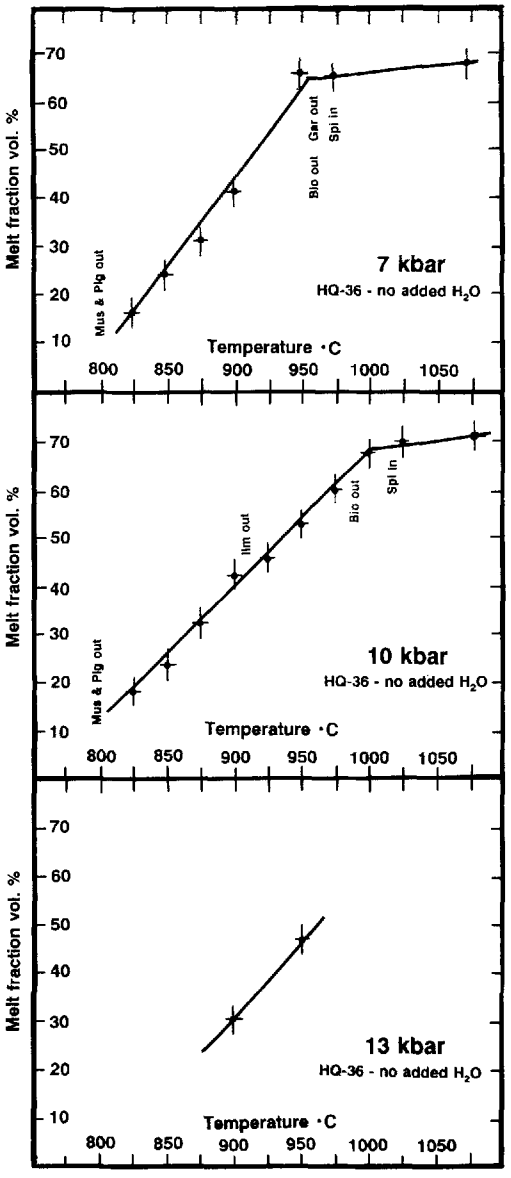

Fig. 3. Vapor-absent melt productivities (vol%) of HQ-36 at *7*, *10* and *13 kbar*. *Straight lines* approximated by eye

tion-melting occurred by reaction (1), the liquid produced should also project on this join. The facts that the liquid (L_1 in Fig. 4a) is considerably richer in H_2O than any point along this join and that alkali feldspar (cf. Thompson and Algor 1977) is not produced in our experiments by the muscovite dehydration-melting reaction, indicate that biotite has also contributed H_2O to the melt in addition to that made available by the breakdown of muscovite. Changes in biotite composition (Patiño Douce and Johnston, in preparation) suggest that this mineral undergoes progressive dehydroxylation with increasing temperature. Thus, our results show that muscovite dehydration-melting in a metamorphic rock containing both muscovite and biotite is more appropriately represented by the following reaction:

$$\text{Mus} + \text{Bio}_1 + \text{Plg} + \text{Qtz} = \text{Bio}_2 + \text{Als} + \text{Melt} \quad (2)$$

where Bio_2 stands for biotite which is less hydrous than that in the initial composition, Bio_1. This reaction is completed at a temperature of at most 800–820° C at 10 kbar.

Although it would be desirable to study reaction (2), which defines the solidus of a metapelitic rock under vapour-absent conditions, direct experimental access to it with our starting material is hampered by two factors. These are the very sluggish kinetics at such relatively low temperatures under H_2O-undersaturated conditions and the difficulty in analyzing the very small "pools" of melt (less than 1 μm across, cf. Fig. 2) formed in HQ-36 at low melt fractions.

Biotite dehydration-melting reaction

In our experiments at 10 kbar biotite reacts out over a temperature interval of at least 150° C (825–975° C, see Table 2), with the melt fraction increasing smoothly over this interval (Fig. 3). In Fig. 5 we show the variation of the modes in this temperature range, calculated relative to the mode at 825° C. This variation is consistent with the following continuous dehydration-melting reaction occurring over this temperature interval:

$$\text{Bio} + \text{Als} + \text{Qtz} \pm \text{Ilm} = \text{Melt} + \text{Gar} \pm \text{Rut} \quad (3)$$

The liquid compositions formed by this reaction are plotted in Figs. 6 and 7. Figure 6 (circles) shows the projection of the peritectic path followed by these liquids on the $Na_2O \cdot Al_2O_3 - K_2O \cdot Al_2O_3 - (MgO + FeO^*)$ (NKM) pseudoternary plane (the base of Fig. 4b). This reaction path clearly shows one of the most important characteristics of the incongruent dehydration-melting reaction (3), namely, that the orthoclase component of biotite enters the melt, whereas its ferromagnesian components, together with those of ilmenite, predominantly combine with aluminosilicate and quartz to form garnet.

The liquids formed by reaction (3) are notably silicic (30–40 wt% normative quartz) and felsic (< 3 wt% $FeO^* + MgO + TiO_2$). Of particular interest is the observation that the reaction relationship between melt and garnet buffers the magnesium and iron contents of the liquid to very low and essentially constant values over a temperature range of about 150° C. This behaviour agrees with the very limited solubility of ferromagnesian phases in silicic melts (e.g. Naney 1983; Puziewicz and Johannes 1988, 1990; Clemens and Wall 1981).

The content of normative corundum in the liquids formed by reaction (3) increases with temperature. Because all of our experimental runs are saturated with aluminosilicate, this increase reflects the temperature dependence of the solubility of excess alumina in granitic melts. Our results confirm (cf. Thompson and Algor 1977; Dimitriadis 1978) that the solubility of excess alumina in H_2O-undersaturated granitic melts is low, amounting to only about 2 wt% Al_2O_3 at 825° C and at most 4–5 wt% Al_2O_3 at 950–1000° C.

An expected consequence of the limited solubilities of Al_2O_3, MgO, FeO and TiO_2 in silicic melts is that

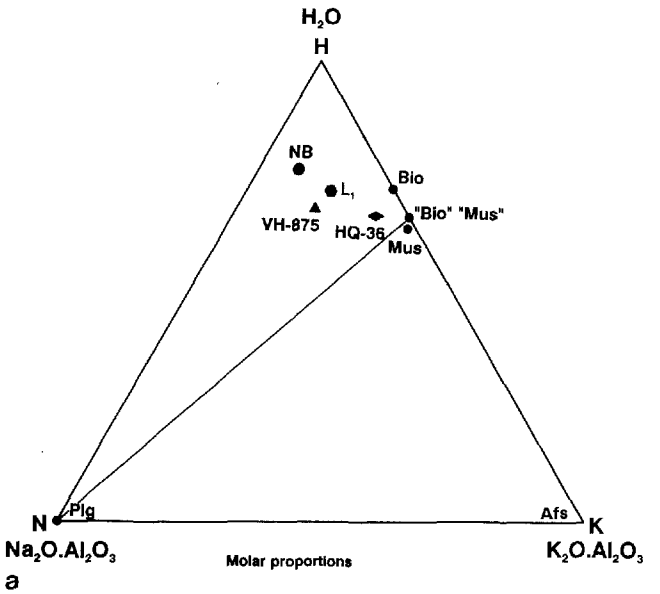

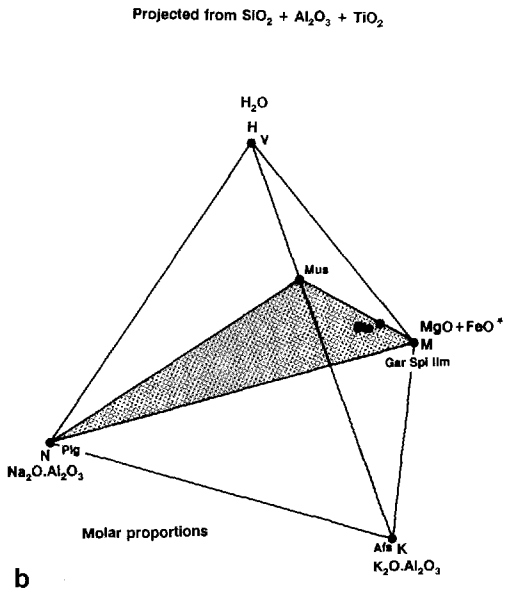

Fig. 4. a NKH pseudoternary projection showing the bulk composition of *HQ-36*, the compositions of micas in HQ-36 (*bio, mus*) and the compositions of stoichiometric micas (*"bio", "mus"*). L_1 is the liquid produced in our 10 kbar, 825° C experiment. *VH*-875 is the liquid reported by Vielzeuf and Holloway (1988) at 10 kbar and 875° C. *NB* is a hypothetical liquid composition at 10 kbar and 725° C, estimated from Nekvasil and Burnham (1987, Figs. 8, 9) and Clemens and Vielzeuf (1987, Fig. 2; a_{H2O} in this melt $\approx$0.7). The spread between these three liquid compositions suggests that the $H_2O/K_2O/Na_2O$ ratios of low-temperature, H_2O-undersaturated granitic liquids are not uniquely determined by pressure and temperature. These melts thus appear to have considerable freedom to accommodate different amounts of K_2O and prevent alkali-feldspar saturation during dehydration-melting (see text). **b** KNMH pseudoquaternary space. Amphibolite-facies metapelitic rocks commonly project on or close to the *shaded plane*. The projection is "legal" because all our runs contain silica-, alumina- and titanium-saturating phases. CaO content is low enough so as not to affect significantly the phase relationships

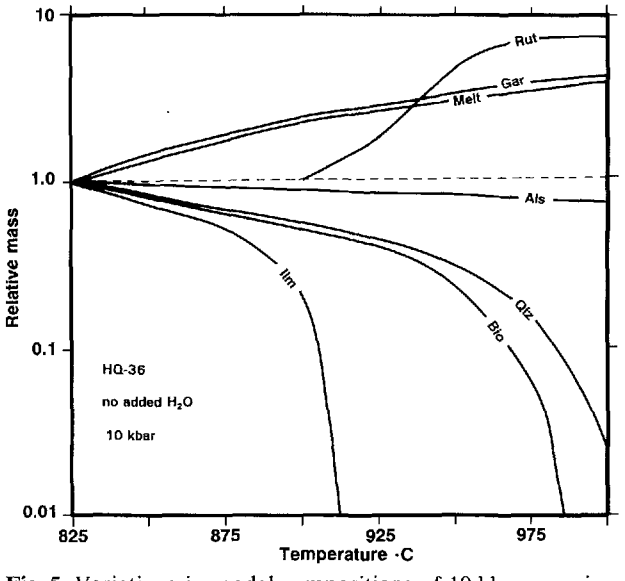

Fig. 5. Variations in modal compositions of 10 kbar experimental run products relative to the mode at 825° C, 10 kbar. Data from Table 5a

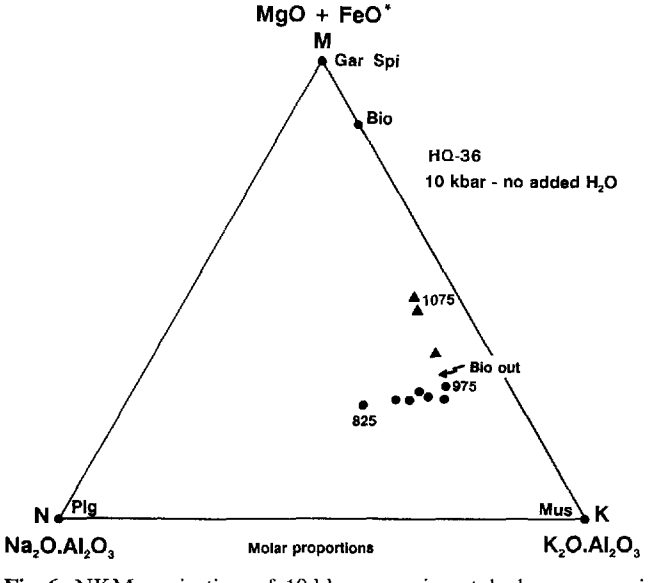

Fig. 6. NKM projection of 10 kbar experimental glass compositions. *Circles* represent glasses that coexist with biotite; *triangles* represent glasses produced above the biotite-out temperature. Numbers next to symbols are temperatures in °C

the compositions of anatectic liquids coexisting with micas should largely be independent of which mica contributed more to their formation. Of the components of micas, orthoclase and H_2O are essential constituents of anatectic silicic melts, whereas excess alumina (in muscovite) and mafic oxides (in biotite) have very limited solubilities in these melts. Hence, the composition of the mica will determine the composition of the restitic phases but should have only a minor effect on the composition of the coexisting melt phase.

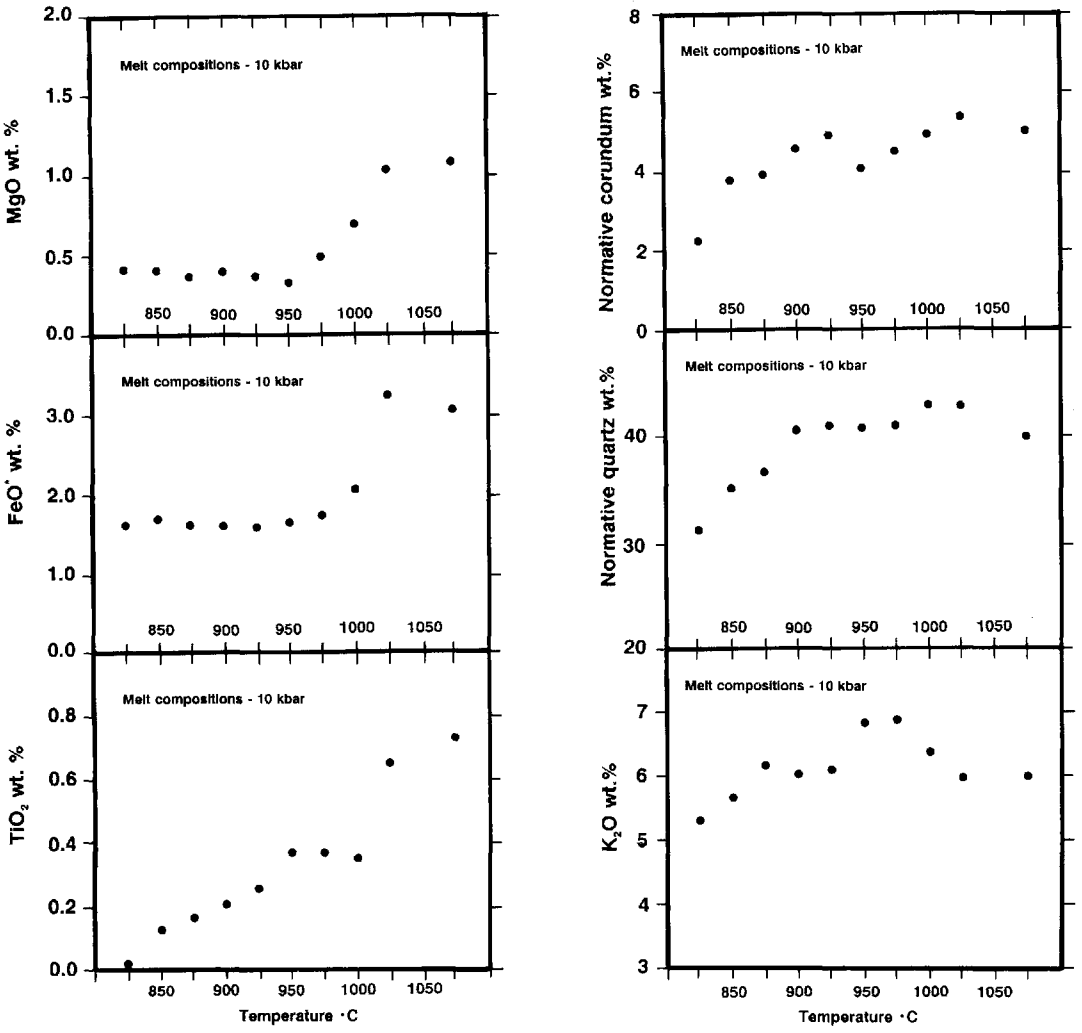

Fig. 7. Compositional variation of glasses produced in 10 kbar experiments. *Points up to 975° C* correspond to reaction (3), whereas *points above this temperature* correspond to reaction (5). Note the different behaviours of the mafic components along these two reactions

Effect of bulk composition on the vapour-absent melting of biotite-bearing assemblages

The observation that liquids formed by dehydration-melting reactions of micas have a narrow compositional range has important consequences for the melting behaviour of metapelitic rocks. The NKM pseudoternary projection in Fig. 8 includes both our melt compositions and those reported by Vielzeuf and Holloway (1988). The proximity between the points representing our 825° C, 10 kbar liquid (L_1) and the lowest-temperature liquid composition reported by Vielzeuf and Holloway (875° C, 10 kbar) suggests that the liquid trend that we observed and that observed by Vielzeuf and Holloway emanate from the same general area, labelled (M) in Fig. 8. This area comprises the compositions of liquids formed largely by muscovite dehydration-melting [with some H_2O contributed by biotite, reaction (2)] but in equilibrium with biotite ± plagioclase before there is any appreciable advance in the biotite dehydration-melting reaction.

Once melt of composition (M) has been generated, subsequent melting is strongly controlled by the bulk composition (and hence the mode) of the protolith. Silica- and alumina-saturated metasedimentary compositions will in general project on, or close to, the biotite-plagioclase join in Fig. 8. The bulk composition studied by Vielzeuf and Holloway lies close to the intersection of this join with that between region (M) and the (MgO + FeO*)vertex (O in Fig. 8). This geometrical relationship implies that the bulk composition chosen by Vielzeuf and Holloway for their experiments is able to generate a large amount of melt of composition similar to that of (M) by the reaction:

$$\text{Bio} + \text{Plg} + \text{Als} + \text{Qtz} = \text{Melt} + \text{Gar} \quad (4)$$

The results of Vielzeuf and Holloway (1988) suggest that reaction (4) is nearly isothermal, generating more than 50 wt% melt over a temperature interval of only 10–20° C. Although it is possible that this sudden increase in melt fraction may in part be a consequence of overstepping reaction (4) in temperature, we argue that the

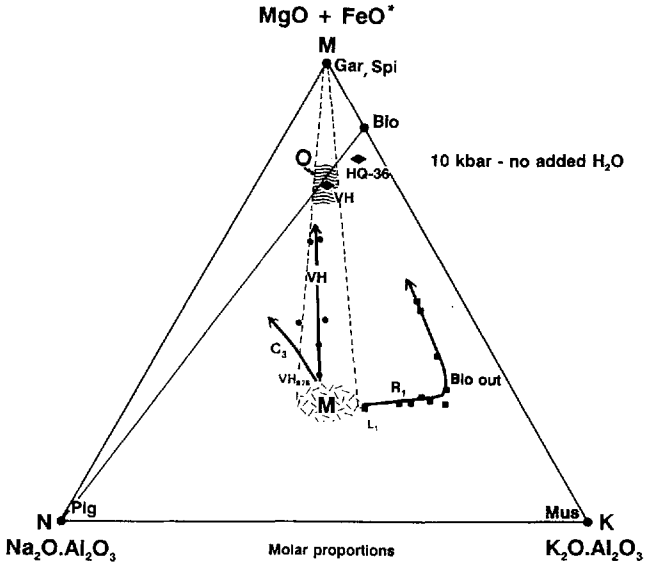

Fig. 8. 10 kbar NKM projection showing our liquid path (*squares*, same as in Figs. 6, 7) and that of Vielzeuf and Holloway 1988 (*circles* labelled *VH*). Anatectic liquids at temperatures approaching the onset of peritectic dehydration-melting reactions of biotite (3 or 4, see text) have compositions within *stippled area M*. Because these reactions produce garnet, and because metapelitic rocks commonly project close to the biotite-plagioclase tie-line, melt production by biotite dehyration-melting will be largest from bulk compositions projecting onto the intersection of this tie-line with the join (*dashed*) between *area M* and the (MgO + FeO*) vertex (*wavy pattern* labelled *O*). The two liquid compositions used to calculate the stoichiometry of the biotite dehydration-melting reaction are L_1 (this study) and *VH875* (Vielzeuf and Holloway 1988). The *diamonds* labelled *VH* and *HQ-36* represent the bulk composition studied by Vielzeuf and Holloway (1988) and that used in this study, respectively

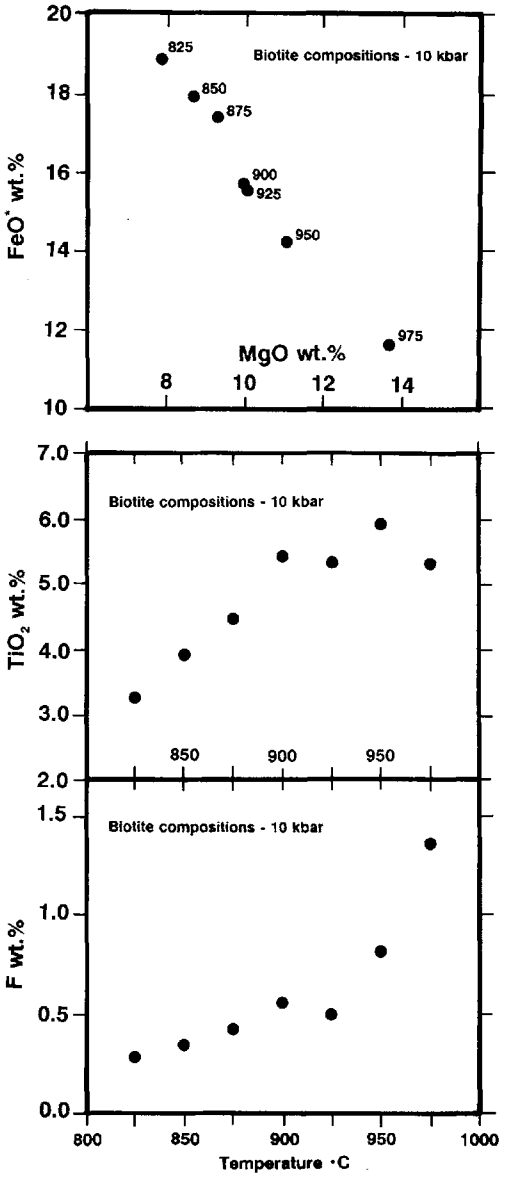

Fig. 9. Compositional variation of biotite in 10 kbar experimental-run products. *Numbers* next to data points in FeO* vs MgO plot are temperatures in °C

compositional relationships shown in Fig. 8 favor the existence of a quasi-isothermal melting step for bulk compositions projecting in the neighbourhood of (O), supporting the results of Vielzeuf and Holloway.

Bulk compositions projecting on the biotite side of (O) (e.g. HQ-36) will, in generating melts of composition (M), exhaust plagioclase before micas and, if temperature can increase significantly in the anatectic region (100° C or more), the liquid composition will subsequently move along reaction path R_1 until biotite is exhausted. The increase in melt fraction takes place in this case over a wide temperature interval (Fig. 3). The actual temperature increase required to consume the excess biotite present in the protolith will depend both on the composition and the amount of biotite in the source material. In our experiments we observe a strong enrichment of TiO_2, F and Mg/Fe in biotite with temperature (Fig. 9 and Patiño Douce and Johnston, in preparation). This observation suggests that the TiO_2 and F contents of the protolith, together with its Mg/Fe ratio, are important factors in determining the maximum temperature-stability of biotite during anatexis.

Bulk compositions plotting on the albite side of (O) (probably more characteristic of metapsammites than of metapelites) will exhaust biotite before plagioclase. The liquid would then presumably follow a cotectic path with a general orientation such as C_3 (see also Fig. 11), dissolving plagioclase and garnet.

Behaviour of alkali feldspar during crustal anatexis

Alkali feldspar is an essential component of granitoid rocks, but it is seldom present in amphibolite-grade metapelitic rocks. Its formation by subsolidus dehydration of muscovite-bearing assemblages at the second sillimanite isograd roughly corresponds to the amphibolite to granulite transition at pressures lower than that of the intersection of this reaction with the wet solidus (point I in Fig. 1). It has heretofore been suggested (e.g. Thompson and Algor 1977; Thompson 1982; Vielzeuf and Holloway 1988) that dehydration-melting reactions at pressures higher than that of this intersection, involving mus-

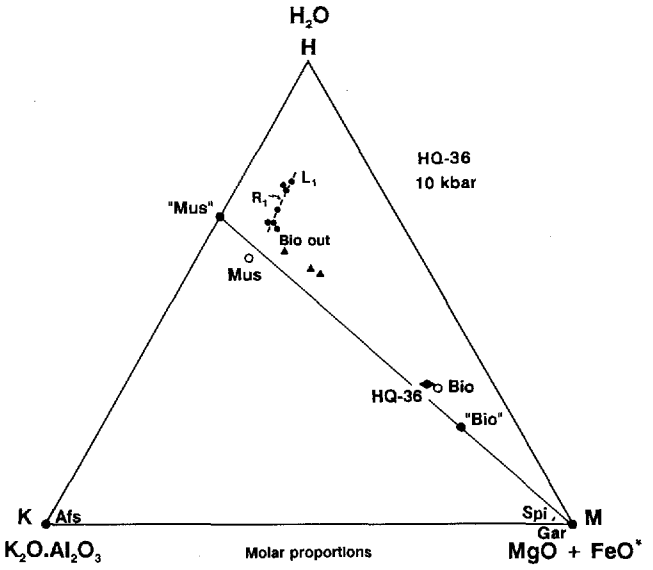

Fig. 10. 10 kbar KMH projection showing the liquid path of our experimental-run products (*circles* for runs containing biotite, *triangles* for runs above the biotite-out temperature). *"Bio", "Mus"*: compositions of stoichiometric micas. *Bio, Mus*: compositions of micas in HQ-36. Bulk composition of HQ-36 shown with *diamond* symbol. Liquids below 900° C have H_2O/K_2O considerably higher than the bulk composition. Because no alkali feldspar is formed by the melting reaction, biotite must undergo progressive dehydroxylation during dehydration-melting reaction (3)

covite or biotite, should also produce alkali feldspar in equilibrium with a granitic liqud. However, alkali feldspar has not been observed as a reaction product in our experiments nor in most other experimental studies of dehydration-melting involving micas and excess quartz (e.g. Sengit and Kennedy 1961; Vielzeuf and Holloway 1988; Peterson and Newton 1989). The experiments of Puziewicz and Johannes (1988) furthermore show that adding a large excess of biotite to a "minimum-temperature" H_2O-saturated haplogranitic liquid increases the K_2O content of the melt and saturates it with mafic phases (cordierite, hercynite, biotite) but not with alkali feldspar. Alkali feldspar was reported as a product of dehydration-melting reactions of biotite by Bohlen et al. (1983) and by Le Breton and Thompson (1988), although in neither case was the identification method stated.

The controls on alkali-feldspar saturation can be addressed with the aid of the $K_2O \cdot Al_2O_3 - (MgO + FeO^*) - H_2O$ (KMH) projection, Fig. 10. Initial liquids formed by dehydration-melting reactions are richer in H_2O than the protoliths from which they are derived (L_1 in Fig. 10). Specifically, the H_2O/K_2O ratio of these liquids is higher than the H_2O/K_2O ratio in micas. With increasing temperature the liquid becomes more anhydros (along peritectic path R_1) and eventually attains the H_2O/K_2O ratio of micas in the protolith. Because all the H_2O is provided by micas during dehydration-melting, H_2O enrichment in the lower-temperature melts requires that a complementary, H_2O-poor phase be generated. The only possibilities are either that mica undergoes progressive dehydroxylation or/and that alkali feldspar is produced by the dehydration-melting reaction. Because the latter is not observed in our experiments, we conclude that biotite becomes more anhydrous. The magnitude of this effect can be appreciated by noting that L_1 requires that about 20 wt% (relative) of the H_2O initially present in biotite be lost at 825° C, and that the liquid at 950° C requires 45% dehydration of biotite. The strong increase in the F content of biotite with temperature (Fig. 9) provides a direct mechanism by which at least part of the proposed dehydroxylation can take place. Titanium enrichment in biotite by an oxy-titanium substitution, thought to be important in granulite-grade metapelitic rocks (e.g. Guidotti 1984; Dymek 1983; Patiño Douce and Johnston, in preparation) can also contribute to biotite dehydroxylation.

Alkali-feldspar saturation will be attained if the maximum stability of mica occurs at a temperature at which the coexisting melt cannot accomodate the orthoclase component of mica. The sum of experimental results cited above, in which alkali-feldspar saturation was not attained at the temperatures at which liquids within the compositional range (M) (Fig. 8) were formed, suggests that the variance of the metapelitic system during dehydration-melting is high enough to allow certain "flexibility" in the $H_2O/K_2O/Na_2O$ ratios of these low-temperature melts (see Fig. 4a). As a consequence, the orthoclase component of micas is able to enter the melt as normative orthoclase and liquids in this temperature range rarely become saturated with alkali feldspar during melting reactions.

Incongruent melting of garnet + aluminosilicate

If the temperature during crustal anatexis exceeds that at which biotite is exhausted, further melting of silica- and alumina-saturated metamorphic rocks involves refractory phases that were either originally present or produced by the mica dehyration-melting reactions: garnet, aluminosilicate, quartz, iron-titanium oxides and, for some bulk compositions, Ca-rich plagioclase. The rate of increase of melt fraction as a function of temperature slows drastically, as shown by the breaks in slope in our melt-productivity curves (Fig. 3), which coincide with the biotite-out temperatures. In general, melting above the biotite-out temperature will not contribute significantly to the volume of anatectic magmas.

The variation in modes above the biotite-out temperature (Table 5) is consistent with the following incongruent-melting reaction:

$$\text{Gar} + \text{Als} = \text{Melt} + \text{Spi} + \text{Qtz} \quad (5)$$

The onset of reaction (5) corresponds to the "elbow" in the liquid path shown in Figs. 6, 8 and 10 (note that the garnet + aluminosilicate melting reaction appears to be cotectic in the NKM and KMH projections, but this is a distortion caused by the coincidence of garnet and spinel in these projections). The main effect of reaction (5) is to enrich the liquid in mafic components. In contrast to the biotite dehydration-melting reaction, the reaction relationship of spinel + quartz with melt does not

appear to have a strong buffering effect on the mafic components of the melt. However, because the increase of melt fraction with temperature caused by the incongruent melting of garnet + aluminosilicate is so small, the liquids remain notably felsic (less than 5 wt% $FeO^* + MgO + TiO_2$) and silica-rich (normative quartz about 40 wt%) up to temperatures of at least 1100° C, at 10 kbar. Temperatures of this order are seldom, if ever, attained during crustal anatexis, whether or not intrusion of basaltic liquids is involved in the process (e.g. England and Thompson 1986; Bergantz 1989; Patiño Douce et al. 1990). Hence, we conclude that anatectic liquids derived from biotite-rich metapelitic sources are always leucogranitic.

Mass balance relations of mica dehydration-melting reactions

The amount of melt of "minimum temperature" composition (M in Fig. 8) produced by dehydration-melting reactions of micas is a function of how close the modal composition of the protolith is to the stoichiometric proportions of reactants required by the melting reaction, and not just of the hydrous-mineral content of the protolith, as often assumed. Most natural aluminous metamorphic rocks contain both muscovite and biotite. If a protolith contains a small amount of muscovite, a small fraction of liquid of composition within region M (Fig. 8) will be generated by muscovite dehydration-melting with some H_2O contribution from dehydroxylating biotite. Assuming that enough H_2O is made available in this fashion, the composition of liquid L_1 (taken as representative of region M) can be generated by balancing reaction (2) as follows:

$$1\text{ g Mus} + 0.50\text{ Plg} + 0.59\text{ g Qtz} + 0.04\text{ g } H_2O\text{ (from Bio)} = 1.77\text{ g Melt} + 0.36\text{ g Als} \quad (6)$$

where the actual composition of muscovite in HQ-36 in used (Table 1), and albite and anorthite are combined in the same proportion as they are present in plagioclase in HQ-36.

If we now imagine this dehydration-melting reaction taking place in a pure muscovite-quartz-plagioclase schist, the extra H_2O required to form liquid of composition M must come from dehydration of muscovite. Considering the amount of muscovite required to provide this extra H_2O and the additional silica required to combine with Al_2O_3 in this muscovite as Al_2SiO_5, the stoichiometry is modified as follows:

$$1\text{ g Mus} + 0.22\text{ g Plg} + 0.33\text{ g Qtz} = 0.75\text{ g Melt} + 0.15\text{ g Als} + [0.20\text{ g Als} + 0.45\text{ g Afs}] \quad (7)$$

The aluminosilicate and alkali feldspar components in square brackets represent the dehydrated muscovite (plus the required amount of silica). All of this aluminosilicate will appear as crystalline aluminosilicate, because liquids in region M are saturated in this phase. Presumably, some of the orthoclase component will enter the melt and some will appear as crystalline alkali feldspar. Even assuming that none of this orthoclase enters the melt, however, this stoichiometry suggests that a pelitic schist devoid of mafic phases, and in which the ratio of muscovite to plagioclase to quartz is that required by reaction 7, should produce about 50 wt% of H_2O-undersaturated melt by vapour-absent melting at a temperature not larger than 800° C. This optimum composition, however, (65 wt% muscovite, 21 wt% quartz and 14 wt% plagioclase) will seldom occur in natural pelitic schists, and the melt productivity of muscovite dehydration-melting reactions will therefore generally be much lower.

In the general case of a protolith with muscovite and biotite we argue that, because the compositions of liquids in equilibrium with biotite + garnet are so restricted, any liquid in the neighbourhood of region (M) (Fig. 8) can be used to estimate the stoichiometry of the biotite + plagioclase dehydration-melting reaction (reaction (4)). For this purpose we have used two different liquid compositions, representative of different portions of region M (Fig. 8): our 825° C, 10 kbar liquid (L_1) and Vielzeuf and Holloway's 875° C, 10 kbar liquid (VH 875). We have assumed also that the biotite composition in HQ-36 is characteristic of biotite from aluminosilicate-bearing metamorphic rocks in the amphibolite facies of metamorphism, and that the plagioclase composition in HQ-36 (An_{25}) is also typical of these rocks. The balanced reactions resulting from these assumptions are the following: For liquid L_1:

$$1\text{ g Bio} + 0.55\text{ g Plg} + 0.14\text{ g Als} + 0.76\text{ g Qtz} = 1.72\text{ g Melt} + 0.73\text{ g Gar} \quad (8)$$

For Vielzeuf and Holloway's 875° C liquid:

$$1\text{ g Bio} + 0.59\text{ g Plg} + 0.26\text{ g Als} + 0.96\text{ g Qtz} = 2.19\text{ g Melt} + 0.62\text{ g Gar} \quad (9)$$

Both reactions predict similar melt productivities: 70 wt% melt in the first case and 78 wt% melt in the second case. The optimum bulk compositions required by both reactions are also similar:

- 41% bio, 23% plg, 31% qtz, 6% Als, for L_1
- 36% bio, 21% plg, 34% qtz, 9% Als, for VH 875

The optimum protolith would resemble a metamorphosed "dirty sandstone" (metagreywacke) rather than a pelitic schist, because of its large plagioclase and quartz contents and relative scarcity of aluminosilicate. A true metapelite, richer in biotite and aluminosilicate than the hypothetical "optimum" described above, but very poor in plagioclase (e.g. HQ-36), will produce far less than 70% melt at temperatures on the order of 870–900° C, showing that rocks of strictly metapelitic composition (i.e. mica schists) are not good source rocks for granitoid magmas (see also Miller 1985; Taylor 1988). Because Na_2O is an essential component of low-temperature silicic liquids, the generation of granitoid magmas with melt fractions exceeding the critical melt fraction (melt fraction at which the magma starts behaving like a fluid, about 50 vol%, Miller et al. 1988) at temperatures not higher than 900° C requires metapsammitic protoliths rich in plagioclase as well as in biotite.

Effect of pressure on melt production from aluminous metasediments

Our experimental results show that there is an observable effect of pressure on melt productivity from aluminous metasediments (Fig. 3) but that this effect is not strong. In general, the melt fraction at a given temperature does not change by more than 15 vol% between 7 and 13 kbar. Melt fractions above the biotite-out temperature, where the melt-productivity curves flatten out, appear to be largely insensitive to pressure.

The melt fractions at 7 and 10 kbar, in the temperature interval 825–900° C, are indistinguishable within the experimental errors (Fig. 3, Table 5), suggesting that biotite dehydration-melting begins at an almost constant temperature within this pressure interval. This observation is consistent with the very steep dP/dT slope of the biotite dehydration-melting reaction at pressures greater than about 6 kbar (e.g. Le Breton and Thompson 1988).

The decrease in melt fraction with increasing pressure at constant temperature that takes place above 900° C is qualitatively consistent with the direct effect of pressure on the solubility of H_2O in silicate melts. The melt-productivity model presented by Clemens and Vielzeuf (1987) is predicated upon this principle and upon the assumption that complex natural systems behave like the haplogranitic system. In particular, they assume that water activity (a_{H2O}) in a dehydration-melting reaction is uniquely determined by the pressure and temperature of melting. These assumptions predict a strong effect of pressure on melt fraction which is not borne out by our experiments. Liquids produced at 7 and 10 kbar have very similar compositions (Table 4), showing that the stoichiometry of the dehydration-melting reaction is largely unaffected by pressure. Because of this we argue that a_{H2O} is not the overriding parameter controlling melt fraction during dehydration-melting. Rather, a_{H2O} will be determined by the stoichiometry of the melting reaction, the activities of the other essential components of granitic melts (quartz, orthoclase and albite) and pressure. This reflects the obvious fact that the variance of natural metapelitic systems is larger than that of the haplogranitic system.

At pressures lower than the range we investigated, the biotite dehydration-melting reaction intersects the garnet-cordierite boundary, and the melting reaction in silica- and alumina-saturated metamorphic rocks becomes (e.g. Grant 1985a; Vielzeuf and Holloway 1988):

$$\text{Bio} + \text{Plg} + \text{Als} + \text{Qtz} = \text{Melt} + \text{Crd} \quad (10)$$

Puziewicz and Johannes (1988) and Green (1976) studied experimentally the equilibrium between peraluminous granitic liquids and cordierite, under H_2O-saturated and undersaturated conditions, respectively. The glass compositions reported in these two studies suggest that the maximum melt fraction generated by reaction (10) lies between 60 and 70 wt%. These values are obviously rough approximations, but they suggest by comparison with the melt productivities reported in this study that a significant increase in melt fraction during decompression is not to be expected. The reason for this is that the solubility of mafic oxides and excess alumina in silica-rich liquids appears to be largely insensitive to pressure and H_2O saturation (compare Table 4 with Puziewicz and Johannes 1988, Table 6 and Puziewicz and Johannes 1990, Table 5). Thus, decompression should not result in significant restite dissolution, even if the liquids become H_2O-saturated.

Discussion and conclusions

Liquidus phase relationships of silica- and alumina-saturated magmas at mid- to deep-crustal pressures

A working model for the vapour-absent, pseudoternary $Na_2O \cdot Al_2O_3 - K_2O \cdot Al_2O_3 - (MgO + FeO^*)$ liquidus phase relationships of silica- and alumina-saturated metamorphic rocks at pressures of 7 to 10 kbar is presented in Fig. 11a. The activity of H_2O is obviously not constant across this phase diagram, which can be thought of as the projection of a curved plane inside the KNMH volume (cf. Fig. 4b). Thus, the relative sizes and shapes of the different liquidus fields are likely distorted, but we believe that the diagram is nevertheless topologically correct. The estimated isotherms are in part constrained by our results and those of Vielzeuf and Holloway (1988) and Le Breton and Thompson (1988).

The two pseudoinvariant points (I_1 and I_2) correspond to the nearly isothermal muscovite and biotite dehydration-melting reactions (2 and 4, respectively). In a pelitic protolith (such as HQ-36) plagioclase is exhausted first at I_1, and with increasing temperature the liquid moves along cotectic C_1, dissolving muscovite and biotite. If muscovite is exhausted next, the liquid dissolves biotite, traversing the biotite field until it encounters reaction path R_1 (corresponding to reaction 3), whence biotite-garnet peritectic melting takes over until biotite is exhausted and the liquid enters the garnet-liquidus field. In the case of a psammitic protolith, muscovite is exhaused at I_1 and then the liquid moves along the short cotectic path C_2 until garnet precipitation begins at reaction point I_2 (reaction 4). A large fraction of low-temperature H_2O-undersaturated peraluminous granitic melt can be generated in the neighbourhood of this pseudoinvariant point (M in Fig. 8) from protoliths of optimum composition.

The phase relationships shown in Fig. 11 assume that the TiO_2 and F contents of the rock are large enough to stabilize biotite along the biotite-garnet peritectic (R_1) to temperatures of about 950° C (e.g. HQ-36). If the bulk composition of a rock is such that the biotite-out temperature is considerably lower, alkali feldspar could be formed during dehydration melting and reaction path R_1 would be truncated by a garnet-biotite-alkali feldspar reaction point leading to an alkali-feldspar liquidus field.

The effect of excess H_2O during anatexis and the different evolutionary paths of anatectic liquids during melting and crystallization can be appreciated in the KMH projection (Fig. 11b). The trace of the plane of

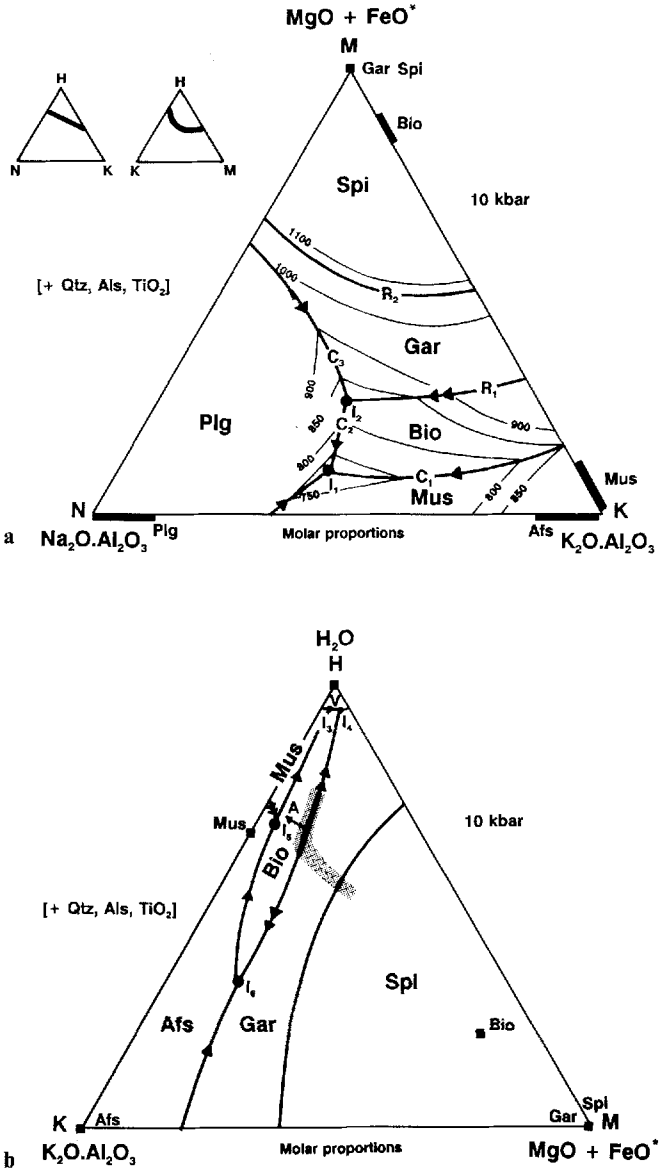

Fig. 11. a (*Top*) Proposed NKM pseudoternary liquidus phase relations for silica-, alumina- and titania-saturated metamorphic rocks at 10 kbar. This diagram is the projection of a curved plane within the KNMH volume, whose traces on the NKH and KMH planes are shown in the *two small triangles*. Isotherms are inferred from our results and those of Vielzeuf and Holloway (1988) and Le Breton and Thompson (1988). **b** (*Bottom*) Schematic KMH pseudoternary liquidus phase relations for silica-, alumina- and titania-saturated metamorphic rocks at 10 kbar. *Stippled pattern* corresponds to our 10 kbar liquid path (see Fig. 10). The existence of a thermal divide on the biotite-garnet reaction depends on the maximum thermal stability of biotite. For bulk compositions poor in TiO_2 and/or F, the biotite field could shrink sufficiently to move reaction point I_6 to more H_2O-rich compositions, eventually eliminating the thermal divide

Fig. 11a projected onto the KMH face of the KNMH volume (mapped by our 10-kbar-liquid compositions) is shown in Fig. 11b with a stippled pattern. These compositions map a protion of the biotite-garnet reaction on the KMH pseudoternary phase diagram and suggest the approximate location of the garnet-to-spinel reaction. The rest of this phase diagram is schematic. Note that the phase relationships shown in Fig. 11b do not include plagioclase, or, in other words, that they are not projected from inside the KNMH volume but represent the Na_2O-free phase relationships on the KMH bounding plane. This does not affect the general principles involved, but simplifies considerably the geometric representation.

If melting of silica- and alumina-saturated metamorphic rocks takes place in the presence of a free H_2O-vapour phase, reaction points I_1 and I_2 (Fig. 11a) are replaced by reaction points I_3 and I_4 in Fig. 11b ($\pm$plagioclase). In this case the first liquid will be generated, at approximately 630° C (at 10 kbar, e.g. Johannes 1984), at reaction point I_3, but the melt will remain there only as long as there is enough H_2O to saturate it at the pressure of melting. Once H_2O is exhausted, the temperature must increase in order for the melt to move along the muscovite-biotite cotectic [or muscovite-biotite-plagioclase inside the KNMH volume, reaction (2)]. If muscovite is exhausted next along this cotectic, the liquid will traverse the biotite field dissolving biotite until the biotite-garnet reaction (3) or the plagioclase-biotite-garnet reaction (4) is encountered.

The contrasting behaviours of alkali feldspar during anatexis and crystallization can also be understood with the aid of Fig. 11b. During anatexis of aluminous metamorphic rocks liquids remain on the biotite-garnet peritectic up to the biotite-out temperature. If garnet is fractionated from the anatectic magma, falling temperature during crystallization will cause the liquid to abandon the biotite-garnet peritectic and the relatively small amount of ferromagnesian components in the melt will crystallize biotite, moving the liquid composition in the general direction A in Fig. 11b [in other words, reaction (3) is prevented from going from right to left]. In so doing, liquids also abandon the plane of Fig. 11a, which hence cannot be used to follow their crystallization. Eventually, and depending on the relative positions of pseudoinvariant point I_5 and of the liquid composition where garnet is fractionated, the cooling melt will reach either the biotite-muscovite or the biotite-alkali feldspar cotectic. In the first case crystallization will proceed towards the vapour-saturated invariant point I_3. In the second case alkali-feldspar saturation is attained first, but cotectic precipitation of alkali feldspar and biotite can give way to subsequent dissolution of alkali feldspar and precipitation of biotite + muscovite once the liquid reaches I_5.

Although the actual position of I_5 is not known, it must move towards more H_2O-rich compositions with decreasing pressure, eventually causing the disappearance of the muscovite field at the pressure (about 3 kbar, e.g. Thompson 1982) at which the muscovite dehydration-melting reaction intersects the H_2O-saturated solidus (muscovite and melt cannot coexist in equilibrium below this pressure, cf. Fig. 1).

The expansion of the alkali-feldspar field at the expense of the muscovite field with falling pressure can have notable effects on the crystallization history of anatectic magmas, depending on the relative rates of cooling and ascent (decompression). For example, if initial cool-

ing takes place at a depth at which the muscovite + biotite ± plagioclase cotectic is encountered first, and that is followed by a rapid decompression (e.g. during a tectonic unroofing event), the early-formed muscovite will be resorbed, together with some biotite, at reaction point I_5, precipitating alkali feldspar. On the other hand, cooling and ascent can proceed simultaneously at rates such that the liquid spends most of its evolution along the alkali feldspar + biotite (± plagioclase) cotectic. We propose that alkali-feldspar megacrystic peraluminous granitoids may originate in this manner.

Comparison of Fig. 11a with b also shows that the crystallizing mineral assemblage is both more felsic and more anhydrous than the melting mineral assemblage. As a consequence water tends to be concentrated in the latest liquids during crystallization, to be combined in hydrous minerals in pegmatites or, ultimately, to be lost to the country rocks, e.g. in the form of injection of hydrothermal veins.

Restite separation vs fractional crystallization in peraluminous granitoids

The compositional characteristics of anatectic melts have two important consequences bearing on the interpretation of natural granitoid rocks. First, because the liquids are so felsic, it appears that most strongly peraluminous granitoids contain some amount of entrained restite (e.g. White and Chappell 1977; Chappel et al. 1987). Second, because liquid variability is restricted, restite separation must be an important factor in controlling the variability within and among strongly peraluminous granitoids.

The phase relationships of melting of silica- and alumina-saturated metamorphic rocks (Fig. 11a) show that plagioclase, garnet and biotite, in addition to quartz and aluminosilicate, can be important restitic phases during progressive anatexis of metasedimentary rocks. However, because garnet is produced by biotite dehydration melting, whereas all the other phases are consumed by this reaction, garnet will likely be the predominant restitic phase during mid- to deep-crustal anatexis of alumina-saturated rocks.

Several lines of argument are consistent with the last conclusion, and suggest that a substantial amount of garnet-rich restite must be fractionated from peraluminous anatectic magmas. Fractionation of restitic garnet appears to be necessary for anatectic liquids to follow the crystallization sequences commonly observed in granitoids, because this fractionation prevents much of the orthoclase component in the melt from recombining as biotite during cooling, and leads to alkali-feldspar saturation. Also, the steep, heavy-rare-earth-element (HREE)-depleted RE patterns of strongly peraluminous granitoids (e.g. Shuster and Bickford 1985; Ortega and Gil Ibarguchi 1990) are best explained by garnet fractionation. More generally, the observation that peraluminous granitoids are richer in silica and alkalies and poorer in alumina and mafic components than their putative metasedimentary protoliths requires that fractionation between felsic liquids and mafic aluminous phases (e.g. garnet) take place during crustal anatexis. Direct evidence for the existence of garnet-rich restite is provided by lower-crustal granulite xenoliths from areas where anatexis is known to have occurred (e.g. Hanchar and Miller 1990; Wooden et al. 1990) which match very closely the restite composition generated in our experiments. Of course, some degree of liquid evolution by fractional crystallization and/or progressive melting (e.g. Grant 1985b) will always be superimposed on restite separation, but we argue that fractionation of restite is the overriding factor in granite evolution.

The actual physical mechanism by which separation of liquid from restite takes place remains elusive, but this does not detract from the fact that the petrologic and compositional relationships of melting of crustal rocks require that such separation operate in nature. Rather, we believe that results such as those discussed here must spur the search for a better physical understanding of the restite separation process.

Fertility of crustal rocks as magma sources

The essential components of low-temperature (less than 900° C) granitoid melts are quartz, albitic plagioclase, alkali feldspar and H_2O. Because the compositional range of such melts is restricted, any of these four components can be the parameter limiting production of low-temperature melts. The genertion of large fractions (more than 50%) of anatectic liquids by vapour-absent melting requires assemblages with rather specific proportions of hydrous minerals, quartz and feldspar. Metapelites, although rich in hydrous minerals, also contain, relative to the composition of low-temperature melts, an excess of refractory material (Al_2O_3, MgO, FeO*, TiO_2) with very limited solubility in such melts. As a result, pelitic schists are rather infertile as magma sources during crustal anatexis. Rocks of psammitic derivation (clay-rich feldspathic sandstones or greywackes) appear to be much better protoliths for granitoid magmas than pelitic lithologies.

The possibility of obtaining large fractions of granitoid melts by vapour-absent anatexis of pre-existing granitoid rocks can also be addressed with our results. Peraluminous granites and granodiorites rarely contain more than 15% biotite + muscovite. By comparison, the "ideal" mode which maximizes melt production requires about 30–40% biotite. Granites and granodiorites are therefore too anhydrous to be fertile protoliths for granitoid magmas. Peraluminous mafic tonalites (e.g. Patiño and Patiño Douce 1987), in contrast, can contain up to about 30% biotite + muscovite, and quartz and plagioclase concentrations comparable to those of the "ideal" composition, suggesting that they can readily re-melt to yield mobile granitoid magmas.

Acknowledgements. We thank Harve Waff for his kindness and generosity in allowing us to use (abuse?) his exerpimental facilities (especially The Anatector) and Jack Rice for providing the rock used for this study as well as useful information on its geologic setting. AEPD thanks Marta Patiño for her support and for getting him involved with granites. Helpful comments from Mike Carroll,

Calvin Miller and Alan Thompson are greatly appreciated. We also thank Steve Wickham, Robert Newton and an anonymous reviewer for their constructive criticism and their help in improving the organization of this manuscript. This work was funded by NSF grants EAR-8720150 and EAR-8915624 to A.D. Johnston. The microprobe facility at the University of Oregon was funded by NSF grant EAR-8803960 and a matching grant from the Keck Foundation.

Appendix

Symbols used in the text

Qtz = quartz	Gar = garnet
Als = aluminosilicate	Spi = hercynitic spinel
Plg = plagioclase	Ilm = ilmenite solid solution
Afs = alkali feldspar	Rut = rutile
Bio = biotite	Crd = cordierite
Mus = muscovite	Hm = haematite

References

Bergantz GW (1989) Underplating and partial melting: implications for melt generation and extraction. Science 245:1093–1095

Bohlen SR (1984) Equilibria for precise pressure calibration and a frictionless furnace assembly for the piston-cylinder apparatus. Neues Jahrb Mineral Monatsh H.9:404–412

Bohlen SR, Boettcher AL, Wall VJ, Clemens JD (1983) Stability of phlogopite-quartz and sanidine-quartz: a model for melting in the lower crust. Contrib Mineral Petrol 83:270–277

Burnham CW (1979) The importance of volatile constituents. In: Yoder HS (ed) The evolution of the igneous rocks. Princeton University Press, Princeton, pp 439–482

Carroll MR, Wyllie PJ (1990) The system tonalite-H_2O at 15 kbar and the genesis of calc-alkaline magmas. Am Mineral 75:345–357

Chappel BW, White AJR, Wyborn D (1987) The importance of residual source material (restite) in granite petrogenesis. J Petrol 28:1111–1138

Clemens JD, Vielzeuf D (1987) Constraints on melting and magma production in the crust. Earth Planet Sci Lett 86:287–306

Clemens JD, Wall VJ (1981) Origin and crystallization of some peraluminous (S-type) granitic magmas. Can Mineral 19:111–131

Didier J (1973) Granites and their enclaves: the bearing of enclaves on the origin of granites. Elsevier, Amsterdam

Dimitriadis S (1978) Some liquid compositions in the peraluminous haplogranite system. Neues Jahrb Mineral Monatsh H.8:377–383

Dymek RF (1983) Titanium, aluminum and interlayer cation substitutions in biotite from high-grade gneisses, West Greenland. Am Mineral 68:880–899

England PC, Thompson AB (1986) Some thermal and tectonic models for crustal melting in continental collision zones. In: Coward MP, Ries AC (eds) Collision tectonics. Geol Soc Spec Publ 19:83–94

Grant JA (1985a) Phase equilibria in partial melting of pelitic rocks. In: Ashworth JR (ed) Migmatites. Blackie, Glasgow

Grant JA (1985b) Decompression melting: an isothermal polybaric liquidus diagram for charnockites (abstract). Geol Soc Am Abstr Program 17:596

Green TH (1976) Experimental generation of cordierite- or garnet-bearing liquids from a pelitic composition. Geology 4:85–88

Guidotti CW (1984) Micas in metamorphic rocks (Reviews in Mineralogy 13). Mineral Soc Am, Washington, DC, pp 357–468

Hanchar JM, Miller CF (1990) Lower crustal xenoliths in Tertiary dikes, Old Woman Mountains area, southaestern California: I. Petrology. Geol Soc Am Abstr Program 22:28

Johannes W (1984) Beginning of melting in the granite system Qz $-$Or$-$Ab$-$An$-H_2O$. Contrib Mineral Petrol 86:264–273

Le Breton N, Thompson AB (1988) Fluid-absent (dehydration) melting of biotite in metapelites in the early stages of crustal anatexis. Contrib Mineral Petrol 99:226–237

Miller CF (1985) Are strongly peraluminous magmas derived from pelitic sedimentary sources? J Geol 93:673–689

Miller CF, Watson EB, Harrison TM (1988) Perspectives on the source, segregation and transport of granitoid magmas. Trans R Soc Edinburgh: Earth Sci 79:135–156

Naney MT (1983) Phase equilibria of rock-forming ferromagnesian silicates in granitic systems. Am J Sci 283:993–1033

Nekvasil H, Burnham CW (1987) The calculated individual effects of pressure and water content on phase equilibria in the granite system. In: Mysen BO (ed) Magmatic processes: physicochemical prinicples. Geochem Soc Spec Publ 1:433–446

Ortega LA, Gil Ibarguchi JI (1990) The genesis of Late Hercynian granitoids from Galicia (northwestern) Spain: Inferences from REE studies. J Geol 98:189–212

Patiño Douce AE, Humphreys ED, Johnston AD (1990) Anatexis and metamorphism in tectonically thickend continental crust exemplified by the Sevier hinterland, western North America. Earth Planet Sci Lett 97:290–315

Patiño MLG, Patiño Douce AE (1987) Petrologia y petrogenesis del Batolito de Achala, provincia de Córdoba, a la luz de la evidencia de campo. Asoc Geol Argent Rev 42:201–205

Peterson JW, Newton RC (1989) Reversed experiments on biotite-quartz-feldspar melting in the system KMASH: implications for crustal anatexis. J Geol 97:465–486

Puziewicz J, Johannes W (1988) Phase equilibria and compositions of Fe$-$Mg$-$Al minerals and melts in water-saturated peraluminous granitic systems. Contrib Mineral Petrol 100:156–168

Puziewicz J, Johannes W (1990) Experimental study of a biotite-bearing granitic system under water-saturated and water-undersaturated conditions. Contrib Mineral Petrol 104:397–406

Rice JM, Grover TW, Lang HM (1988) $P-T$ evolution of the St. Joe-Clearwater region, northern Idaho. Geol Soc Am Abstr Program 20(7):A18

Rutter MJ, Wyllie PJ (1988) Melting of vapour-absent tonalite at 10 kbar to simulate dehydration-melting in the deep crust. Nature 331:159–160

Segnit RA, Kennedy GC (1961) Reactions and melting relations in the system muscovite-quartz at high pressures. Am J Sci 259:280–287

Shuster RD, Bickford ME (1985) Chemical and isotopic evidence for the petrogenesis of the northeastern Idaho batholith. J Geol 93:727–742

Taylor HP (1988) Oxygen, hydrogen and strontium isotope constraints on the origin of granites. Trans R Soc Edinburgh: Earth Sci 79:317–338

Thompson AB (1982) Dehydration melting of pelitic rocks and the generation of H_2O-undersaturated granitic liquids. Am J Sci 282:1567–1595

Thompson AB, Algor JR (1977) Model system for anatexis of pelitic rocks. I. Theory of melting reactions in the system $KAlO_2$ $-NaAlO_2-Al_2O_3-SiO_2-H_2O$. Contrib Mineral Petrol 63:247–269

Vielzeuf D, Holloway JR (1988) Experimental determination of the fluid-absent melting relations in the pelitic system. Consequences for crustal differentiation. Contrib Mineral Petrol 98:257–276

White AJR, Chappell BW (1977) Ultrametamorphism and granitoid genesis. Tectonophysics 43:7–22

Wooden JL, Bennett VC, Hanchar JM, Miller CF (1990) Lower crustal xenoliths in Tertiary dikes, Old Woman Mountains area, southeastern California: II Pb, Nd and Sr isotopic data. Geol Soc Am Abstr Program 22:95

Editorial responsibility: T. Grove